Electronic supplementary information (ESI) for

A chemically stable hydrogen-bonded organic framework for SO_2/CO_2 separation

Jun Liang,[a,b] Shang–Hua Xing,[a,b] Philipp Brandt,[b] Alexander Nuhnen,[b] Carsten Schlüsener,[b] Yang–Yang Sun,[b] and Christoph Janiak*[a,b]

[a] Hoffmann Institute of Advanced Materials, Shenzhen Polytechnic, 7098 Liuxian Blvd, Nanshan District, Shenzhen, China
[b] Institut für Anorganische Chemie und Strukturchemie, Heinrich–Heine–Universität Düsseldorf, Universitätsstraße 1, 40225 Düsseldorf, Germany

Additional Emails: liangj@uni-duesseldorf.de; xingshanghua@126.com; p.brandt@hhu.de; Alexander.Nuhnen@uni-duesseldorf.de; carsten.schluesener@hhu.de; Yangyang.Sun@uni-duesseldorf.de

Table of Contents

S4. Table S1–S7

S5. References

S1. Experimental Details

1. Materials

All starting materials and solvents were obtained from commercial sources. Hydrochloric acid (37 wt%), methanol (99.99%), urea (> 99.5%) were obtained from Sigma–Aldrich. Paraformaldehyde (95–100.5%) was bought from Carl roth. Glyoxal (40 wt% solution in H_2O) was obtained from J&K company.

2. Characterization methods

Powder X–ray diffraction patterns (PXRD). All samples were measured over the *2θ* range of 5 – 50° with a scan speed of 1.5° min^{-1} on a Bruker D2 Phaser powder diffractometer equipped with a flat silicon, low background sample holder using Cu–K*α* radiation (λ = 1.5418 Å, 30 kV, 10 Ma, ambient temperature). Simulated patterns of CB6 H were calculated with CCDC Mercury 3.7 program using the single crystal data (CCDC no. 676880, Refcode KOBNEV).

SEM and TEM. High resolution scanning electron microscopy (SEM) image was recorded with a Jeol JSM–6510LV QSEM Advanced electron microscope with a LAB–6 cathode at 20 keV.

Transmission electron microscope (TEM) images were taken on a FEI TECNAI G2 F20 microscope at an accelerating voltage of 200 kV.

FT–IR. Fourier transform infrared (FT–IR) spectra of samples were recorded on a Bruker FT–IR Tensor 37 as attenuated total reflection in the range of 550–4000 cm^{-1}. For IR measurement on nanoCB6-H with SO_2 adsorbate, nanoCB6-H powder was first degassed at 423 K for 24 hours before the dose of SO_2 by manual up to 350 Torr and held by 10 minutes, then the sample was backfilled with helium. The sample tube with SO_2@nanoCB6-H powder was immediately put in a Dewar bottle with very limited amount of liquid N_2 for a short time (within two minutes) and the sample was poured out to measure IR spectra. For comparison, activated nanoCB6-H without SO_2 adsorption was also treated with the same procedure. SO_2@nanoCB6-H powder was activated under vacuum at 423 K for two hours before the collection of IR spectra of recycled nanoCB6-H again.

NMR. The ^1H NMR was performed at AVANCE III Bruker Biospin spectrometer, operating at 300 MHz. **EA.** Elemental analyses of C, H, and N were carried out on an Elementar Vario EL III analyzer. **TGA**. Thermogravimetric analysis (TGA) were carried out with a Netzsch TG 209 F3 Tarsus in the range of 30 °C to 650 °C with a heating rate of 10 K min^{-1} under oxygen atmosphere.

3. Preparation of nanoCB6-H and CB6-H

For gas sorption by porous adsorbents, it is recognized that the uptake amount can be affected by various factors including the pore size (the critical pore diameter) and overall particle size of the adsorbent material, as each uptake point is related to the equilibrium time at certain partial pressure. If the critical pore diameter of the adsorbent is close to the kinetic diameter of the adsorbate molecule, or the particle size of the adsorbent is relatively large, then this will lower the permeance, and longer equilibrium times are usually needed. Therefore, an uptake by an adsorbent with larger particle size could be under-determined under the same equilibrium time parameters. Taking this into consideration, we have chosen nanoscale particle sizes of CB6-H, termed nanoCB6-H in this work for investigation in order to facilitate the exposure of CB6 cages to SO_2 molecules, and to minimize the diffusion time effect as the portal size of CB6 (3.9 Å) is very close to the kinetic diameter of SO_2 (4.1 Å). micro-size crystallites of CB6-H were also prepared and investigated for comparison.

nanoCB6-H was prepared according to a reported method with modification.[1a] 250 mg CB6 was dissolved in 5 mL 6 M HCl after sonication for two minutes. Then the solution was filtered through membrane (20 um). The obtained CB6 solution was rapidly poured into 25 mL methanol under string at 300 rpm, and kept stirring for two minutes. Transfer the white mixture into a 50 mL centrifugation tube, 5000 rpm for 5 minutes, and the upper solution was removed. 25 mL fresh methanol was added to disperse the solid under sonication, then being centrifugated at 5000 rpm for 5 minutes. This process was repeated one more time. Put the solid product in vacuum oven at 60 ℃ for 12 hours before cooling down to R.T, and grind slightly the product into powder, then put the powder under dynamic vacuum oven at 100 ℃ for 48 hours. Elemental analysis data for nanoCB6-H. Calcd (%) for $C_{36}H_{36}N_{24}O_{12}\cdot 1.8H_2O$: C, 42.01; H, 3.88; N, 32.66. Found: C, 41.94; H, 4.34; N, 31.18. ^{1}H NMR, (300 MHz, D_2O/KCl, 25 °C): δ (ppm) = 5.83–5.78 (d, 12H, N–CH_2–N), 5.72 (s, 12H, –CH–), 4.48–4.43 (d, 12H, N–CH_2–N). FT–IR characteristics (KBr, u_{max}, cm^{-1}): 3471 (w, H_2O), 2999, 2927 (w, C–H), 1734 (w, C=O), 1476 (s, CH_2), 1329 (s), 1236 (s), 1190 (s), 966 (s), 800 (s).

CB6-H was prepared according to previous report,[1c] and characterized by PXRD and N_2 sorption at 77 K (Fig. S32).

4. Gas sorption measurements

SO_2, CO_2, CH_4 and N_2 sorption isotherms for both newly activated and recycled nanoCB6-H materials were recorded at 293 K (water bath with temperature control system) and 273 K (ice/water bath) on a Quantachrome Autosorb IQ MP. Before the measurement, the nanoCB6-H samples were activated at 373 K in vacuum for 48 hours. In control experiments, nanoCB6-H or CB6-H was activated continuously at 423 K in vacuum for 48 hours. All gases were of ultrapure grades (99.999%) supplied by Air Liquide Germany and used as–received.

SO_2 sorption experiments were performed on an Autosorb iQ MP instrument within a pressure range of $1\cdot10^{-3}$–1 bar. For safety precautions of toxic SO_2, a *Dräger Pac 6000* SO_2–detector (0–100 ppm in 0.1 ppm steps) was used in close range to the sorption–device. SO_2–sorption experiments with our setup involve some limitations emerging from the corrosive nature of the SO_2 adsorptive. Each SO_2 sorption run had to be completed within a maximal time of 10 h. This time limit was specified by the Quantachrome company to prevent damage to the gaskets. Irreversible swilling of the SO_2 adsorbing gaskets in the measurement device could cause leaks in the system. Thus, the measurement time (10 hours at maximum) should be set to protect the device. After each measurement, the system had to be regenerated by flushing with nitrogen for at least five times, and remained under N_2 atmosphere for at least 12 hours to regenerate the gaskets. In the case of long equilibration times upon adsorption and desorption, we decided to collect the adsorption data points as complete as possible with long–enough equilibration times at the expense that fewer data points could be measured for desorption. This compromise then led to incomplete, i.e. not–closed desorption branches, which however are solely due to the experimental boundary conditions and cannot be interpreted in terms of decomposition or chemisorption. In SO_2 adsorption recycle experiments, recycled sample was degassed at 373 K under vacuum for at least two hours. For SO_2 adsorption at 353 K conditions, recycled sample after conducting SO_2 adsorption at 293 K for ten runs was used, and an oil batch with temperature control system was set up.

Nitrogen sorption measurements at 77 K were carried out on a Micrometrics ASAP 2020 or Autosorb 6 gas sorption analyzer. Before the measurement, the samples were activated at 373 K in vacuum for 48 hours. The Brunauer–Emmett–Teller (BET) surface areas were calculated based on a few points in the p/p_o range of 0.005–0.08 using the ASAP 2020 v3.05 software. Total pore volumes were calculated from nitrogen

adsorptions isotherms at p/p_o = 0.9. Micropore volumes were calculated based on t–plot method in the p/p_o range of 0.1–0.2. The pore size distributions were obtained using nonlocal density functional theory (NLDFT) calculations with an "N_2–Tarazona, cylinder" model.

S2. Computational details

1. Virial analysis for SO_2

To calculate the isosteric enthalpy of adsorption (ΔH_{ads}) for SO_2 isotherm data, virial method was used. Equation (eq. 1) was used to fit the adsorption data simultaneously at 273 K and 293 K in Origin.

$$\ln(P) = \ln(n) + \frac{1}{T}\sum_{i=0}^{n} a_i n^i + \sum_{j=0}^{m} b_j m^j \qquad (1)$$

In equation (1), P is the pressure in kPa, n is the total amount adsorbed in mmol g^{-1}, T is the temperature in K (here 273K, 293K), a_i and b_i are virial coefficients, and n, m represent the number of coefficients required to adequately fit the isotherms.

Then ΔH_{ads} can be calculated from equation (eq. 2), where R is the universal gas constant.

$$\Delta H_{ads} = -\,Q_{st} = R \sum_{i=0}^{n} a_i n^i \qquad (2)$$

2. IAST calculations[2]

Selectivities of SO_2 over CO_2 of nanoCB6-H were calculated from the dual–site Langmuir (DSL) (eq. 3) fitted isotherm data.

$$q_{eq} = q_{m,1} \cdot \frac{K_1 \cdot p}{1 + K_1 \cdot p} + q_{m,2} \frac{K_2 \cdot p}{1 + K_2 \cdot p} \qquad (3)$$

The 3P sim software (3P Instruments, Germany, version 1.1.0.7) calculates the maximal loadings of each gas depending on the given mole fraction.

IAST selectivities S of binary gas mixtures were calculated using equation 4, where x_i represents the absorbed gas amount and y_i the mole fraction of each adsorptive.

$$S = \frac{x_1/x_2}{y_1/y_2} \qquad (4)$$

Selectivities of SO_2 over CH_4, and SO_2 over N_2 of nanoCB6-H were calculated from the dual–site Langmuir (DSL) (eq. 3) fitted isotherm data. IAST with DSLangmuir isotherm mode was chosen, and the total pressure was fixed at 1 bar to give the IAST selectivity versus the SO_2 molar fractions between 0.01 and 0.5 bar in gas mixtures. Alternatively, SO_2 to CH_4 (or SO_2 to N_2) volume ratio was fixed to give the IAST selectivity vs pressure between 0.1 to 1.0 bar based on eq.4.

3. Molecular simulation

All density functional theory (DFT) calculations were performed with Becke, three-parameter, Lee-Yang-Parr (B3LYP) functional by using Gaussian 16 software.[3] The initial configuration of CB6 was obtained from the single-crystal structure (CCDC no. 676880, Refcode KOBNEV). The geometric optimization of CB6 was carried out at the level of B3LYP/6-311G** method. The same level of method for CB6 geometric optimization was also used on other literatures.[4] The SO_2 molecule was manually placed on the optimized CB6 configuration with different site, and then the fully relax optimizations of complex models SO_2_CB6 were

performed. The binding energy of SO_2 molecule with CB6 was calculated by the dispersion corrected B3LYP-D3 functional[5] along with 6-311G**. The basis set superposition error (BSSE) was corrected by the counterpoise method.[6] The binding energy was thus obtained from the equation 5:

$$E(\text{binding energy}) = E(SO_2\_CB6) – E(CB6) - E(SO_2) + E(BSSE) \quad (5)$$

where $E(SO_2\_CB6)$ corresponds to the total energy of CB6 model with one SO_2 molecule, and E(CB6) and $E(SO_2)$ are the total energies of CB6 model without SO_2 and only one SO_2 molecule, respectively.

4. Breakthrough simulations

Breakthrough simulations were calculated using 3P sim software. The calculations were based on a 30 cm high column with an inner diameter of 3 cm, axial dispersion of 50 $cm^2\ min^{-1}$ and a continuous gas flow of 20 $mL\ min^{-1}$. Generally mass transfer coefficients in our dispersion model were set to 10 min^{-1} for all gases.

S3. Fig. S1–S31

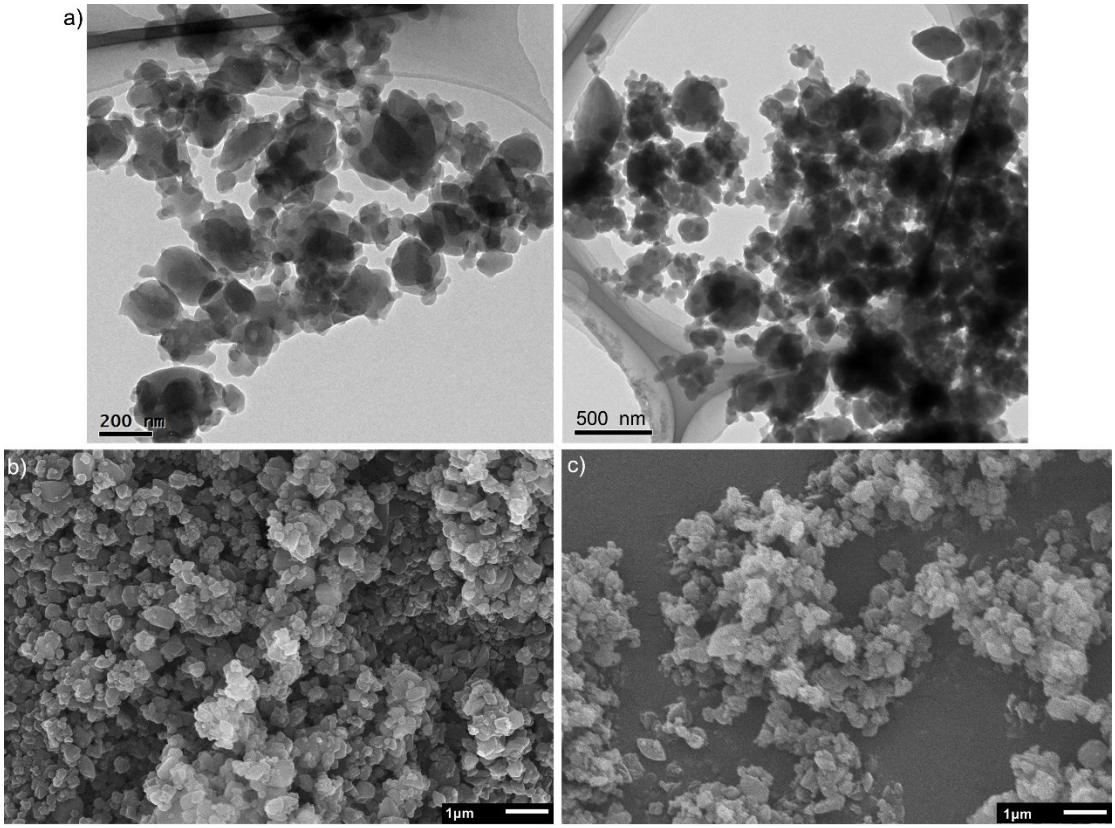

Fig. S1 a) TEM images of nanoCB6-H with different magnification. SEM images of nanoCB6-H b) before and c) after SO_2 uptake at 293 K up to 0.97 bar.

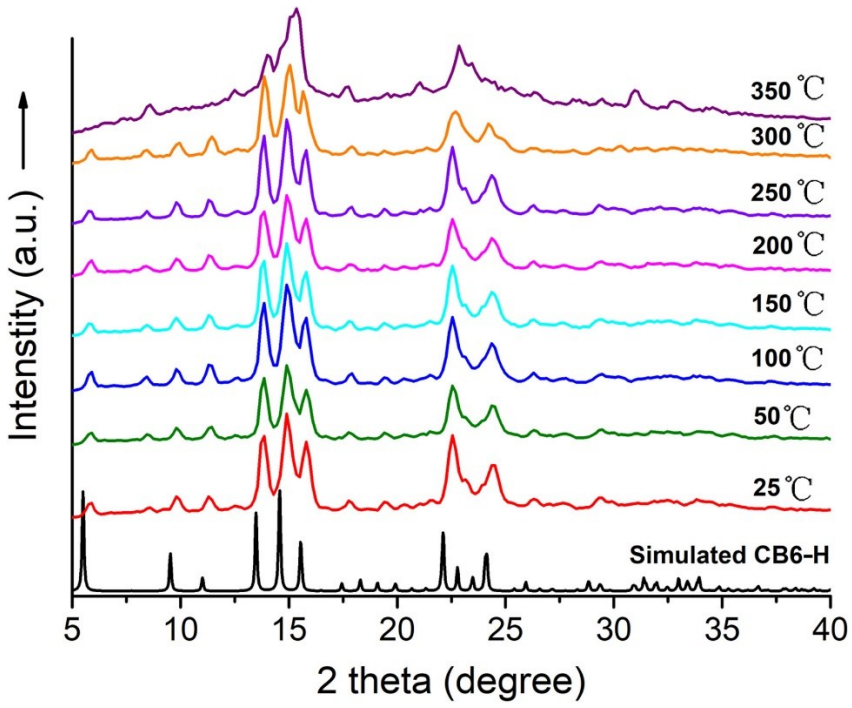

Fig. S2 PXRD patterns of nanoCB6-H at different temperature under air.

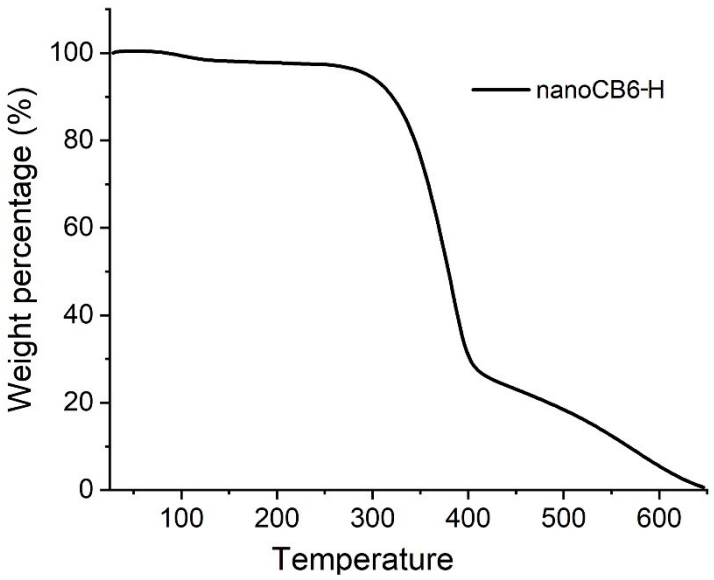

Fig. S3 TGA curve of nanoCB6-H at different temperature under oxygen atmosphere.

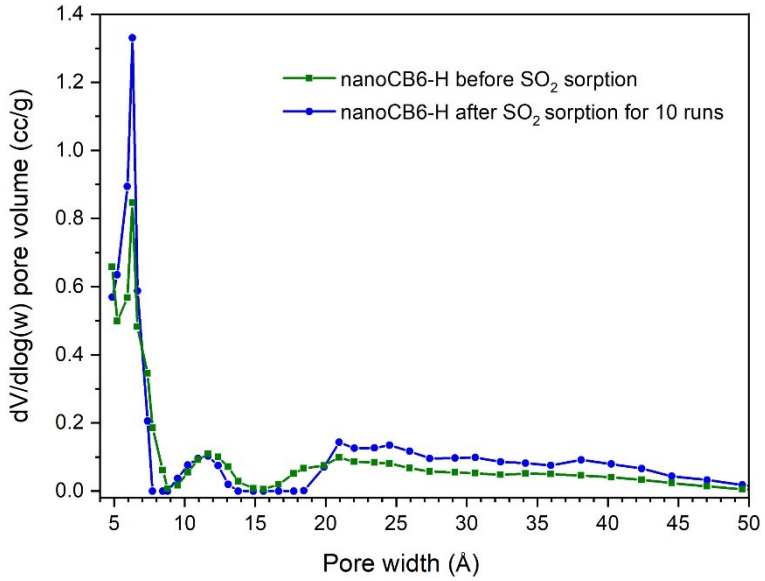

Fig. S4 The pore size distributions of nanoCB6-H before SO_2 sorption (green) and after ten runs of SO_2 sorption (blue).

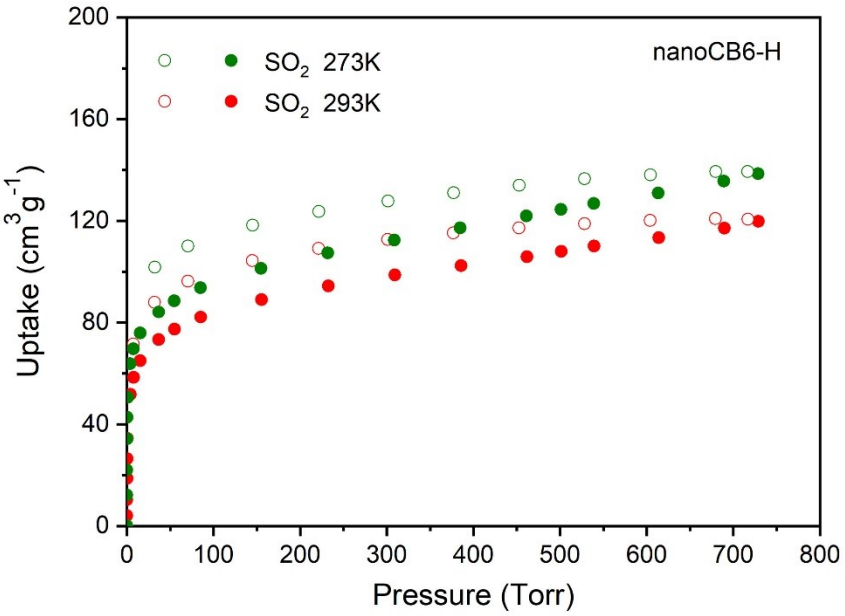

Fig. S5 SO_2 uptake isotherms (the 7th and 8th runs) of recycled nanoCB6-H measured up to 1 bar at 293 K and 273 K, respectively. Filled and empty symbols represent adsorption and desorption, respectively.

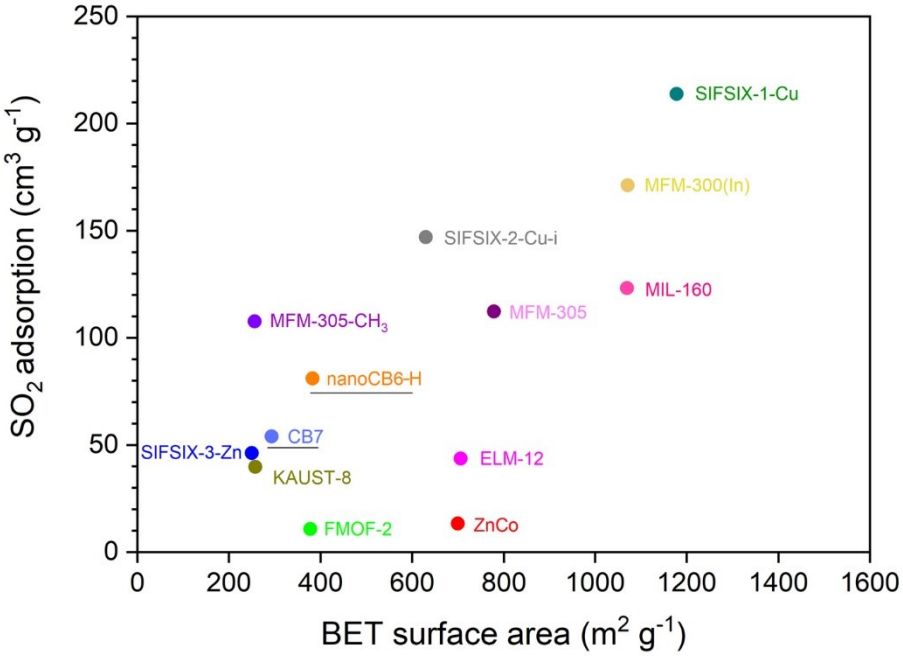

Fig. S6 Comparison of SO_2 uptakes of nanoCB6-H and representative MOFs at 0.1 bar. Plot of SO_2 adsorption (at 0.1 bar and 298 K) against BET surface area. Temperature for nanoCB6-H and MIL–160 is at 293 K. Cage involved materials are underlined.

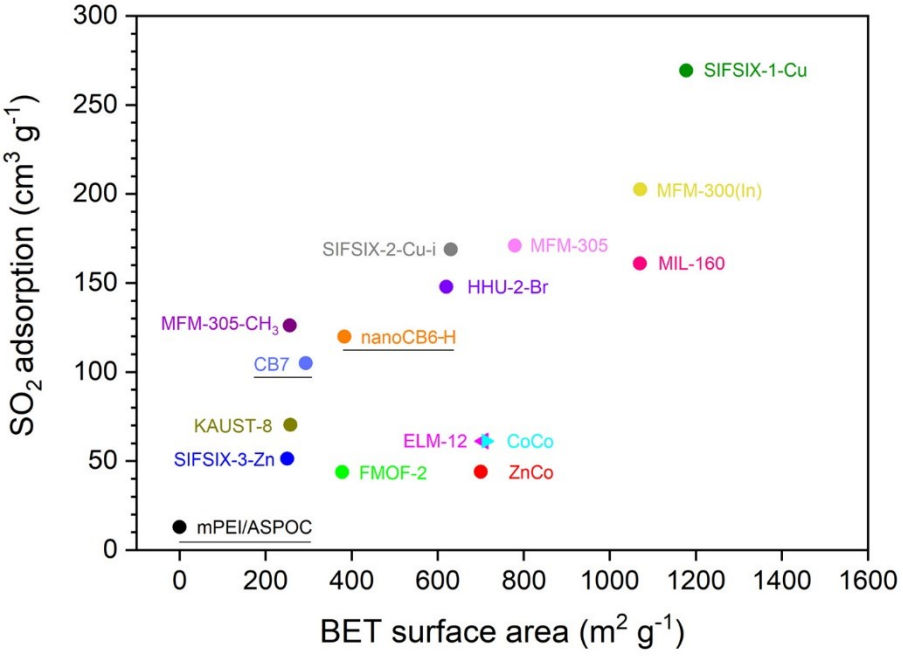

Fig. S7 Comparison of SO_2 uptakes of nanoCB6-H and representative MOFs at 1.0 bar. Plot of SO_2 adsorption (at 1.0 bar and 298 K) against BET surface area. Temperature for nanoCB6-H and MIL–160 is at 293 K. Cage involved materials are underlined.

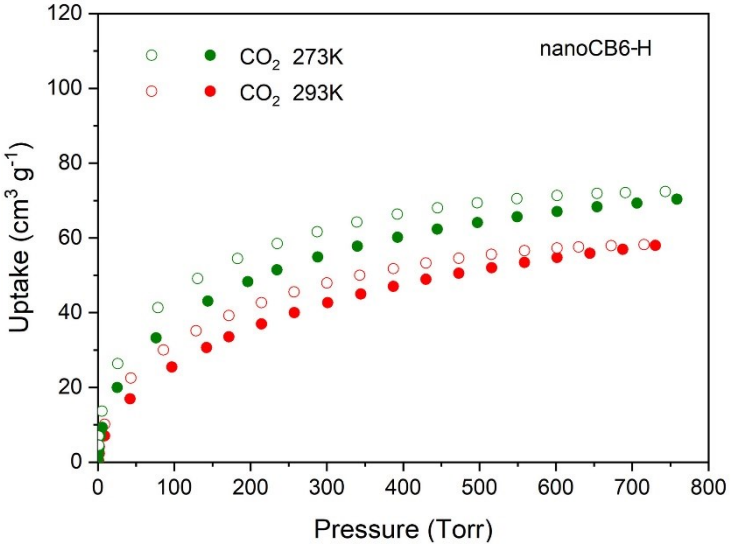

Fig. S8 CO_2 uptake isotherms of recycled nanoCB6-H measured up to 1 bar at 273 K and 293 K, respectively. Filled and empty symbols represent adsorption and desorption, respectively.

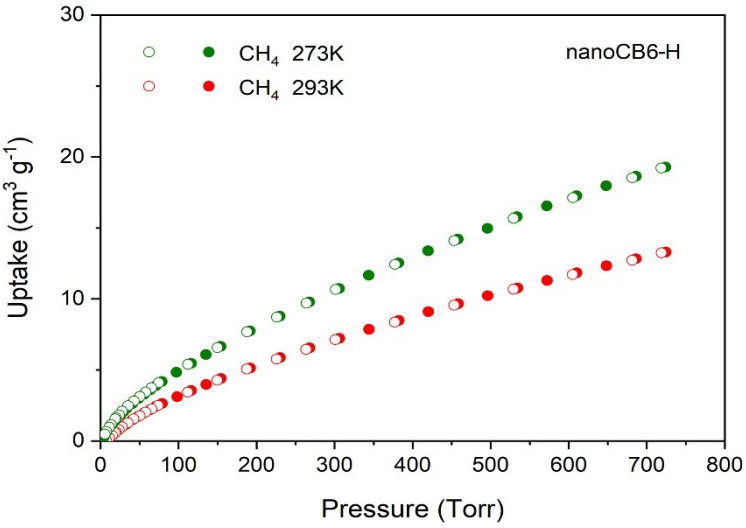

Fig. S9 CH_4 uptake isotherms of nanoCB6-H measured up to 1 bar at 273 K and 293 K, respectively. Filled and empty symbols represent adsorption and desorption, respectively.

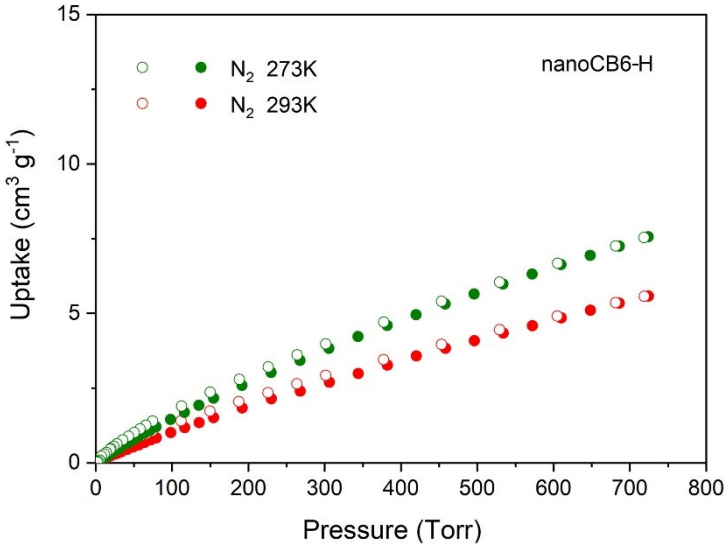

Fig. S10 N_2 uptake isotherms of nanoCB6-H measured up to 1 bar at 273 K and 293 K, respectively. Filled and empty symbols represent adsorption and desorption, respectively.

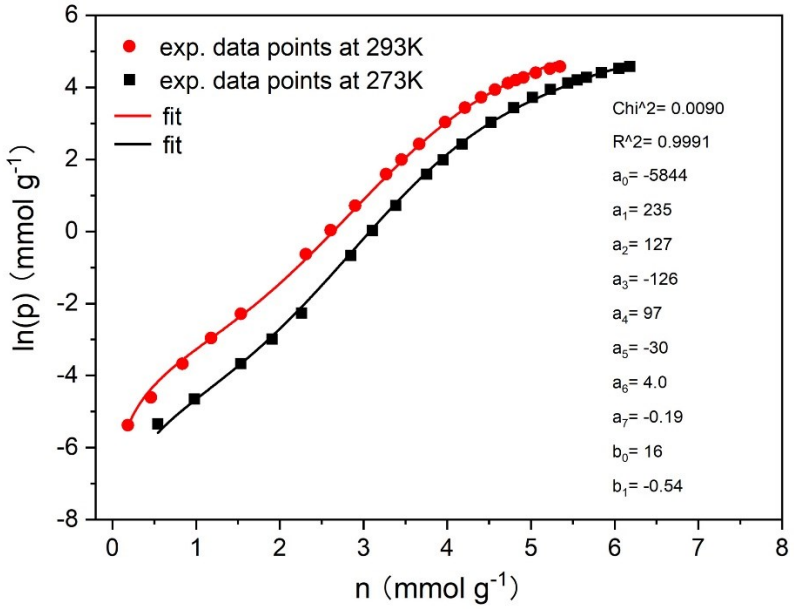

Fig. S11 Virial analysis of the SO_2 sorption data for recycled nanoCB6-H.

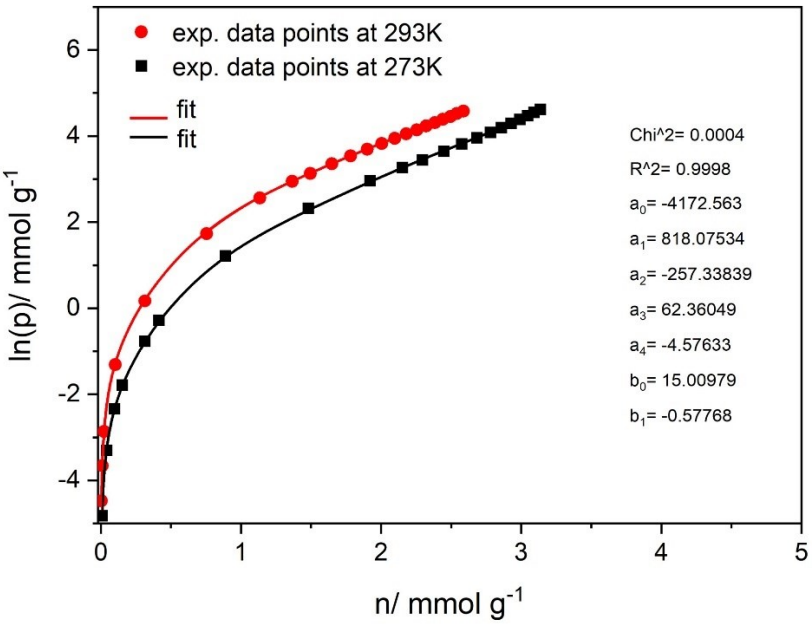

Fig. S12 Virial analysis of the CO_2 sorption data for recycled nanoCB6-H.

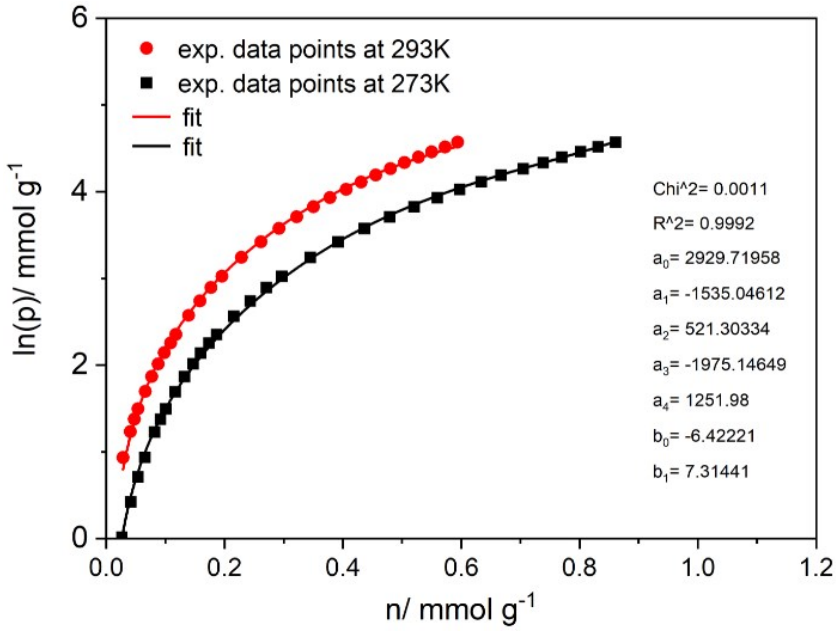

Fig. S13 Virial analysis of the CH_4 sorption data for nanoCB6-H.

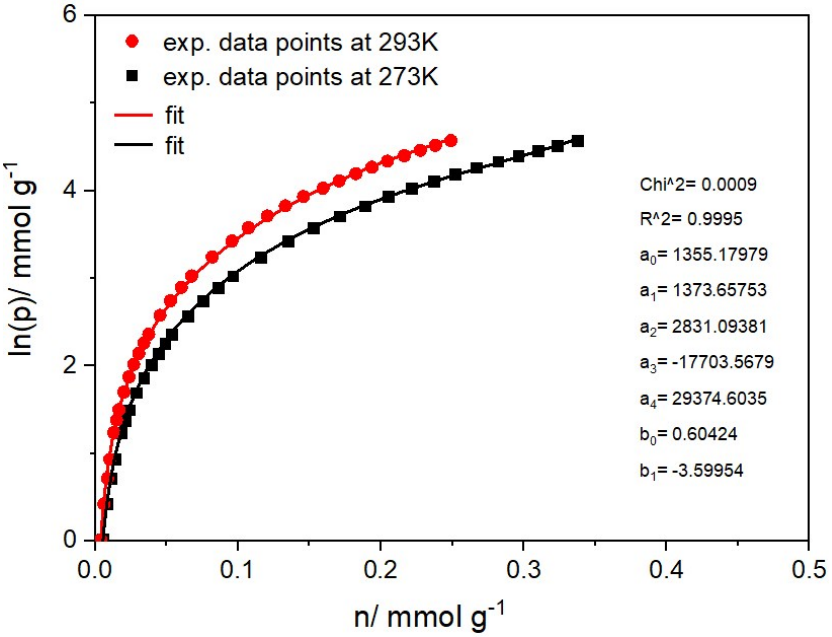

Fig. S14 Virial analysis of the N_2 sorption data for nanoCB6-H.

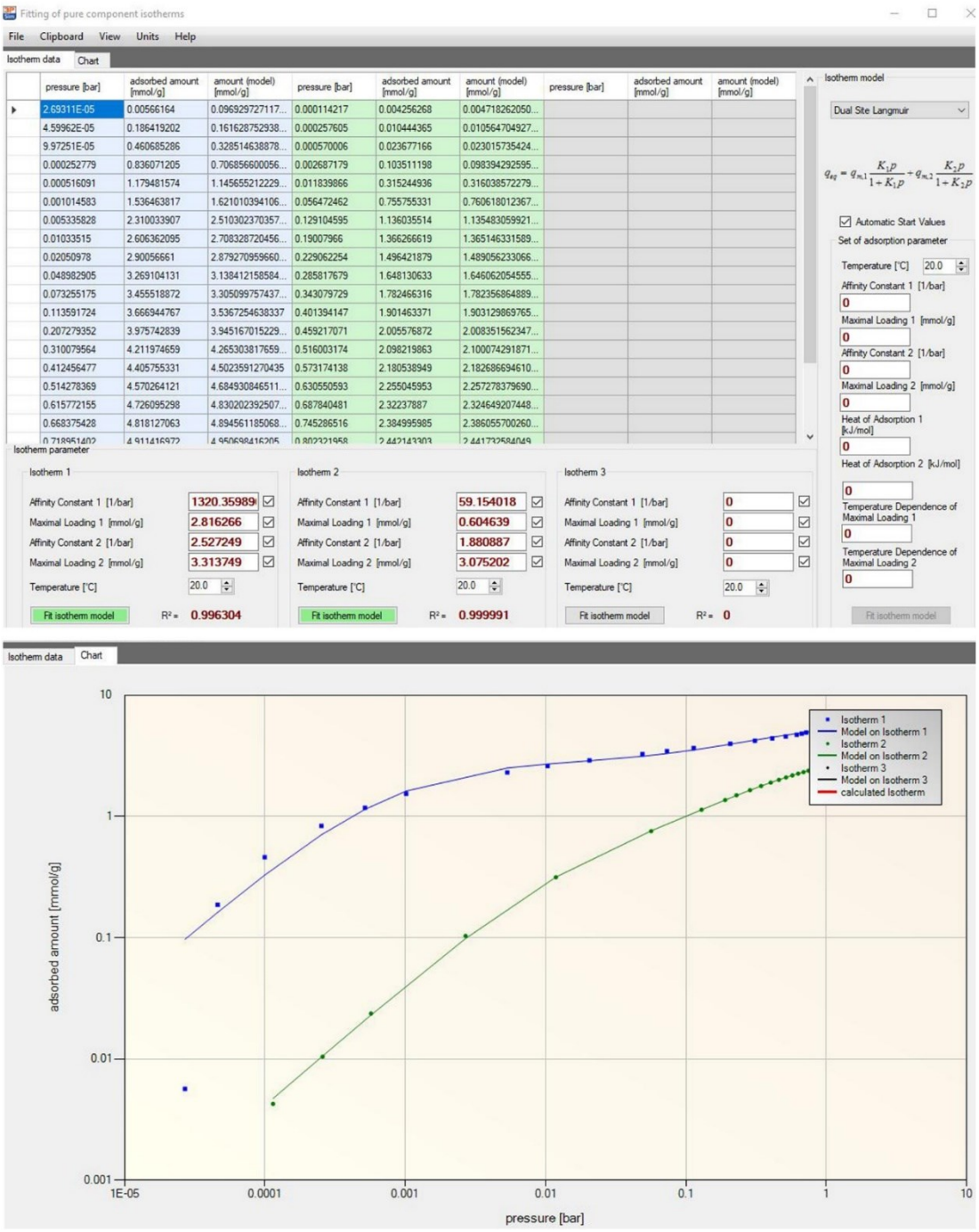

Fig. S15 The automatic isotherm parameters of SO_2 (blue curve) and CO_2 (green curve) fitted by the Dual Site Langmuir (DSLAI) model (top). The corresponding fitting results of chart with log(x) and log(y) for better visualization (bottom).

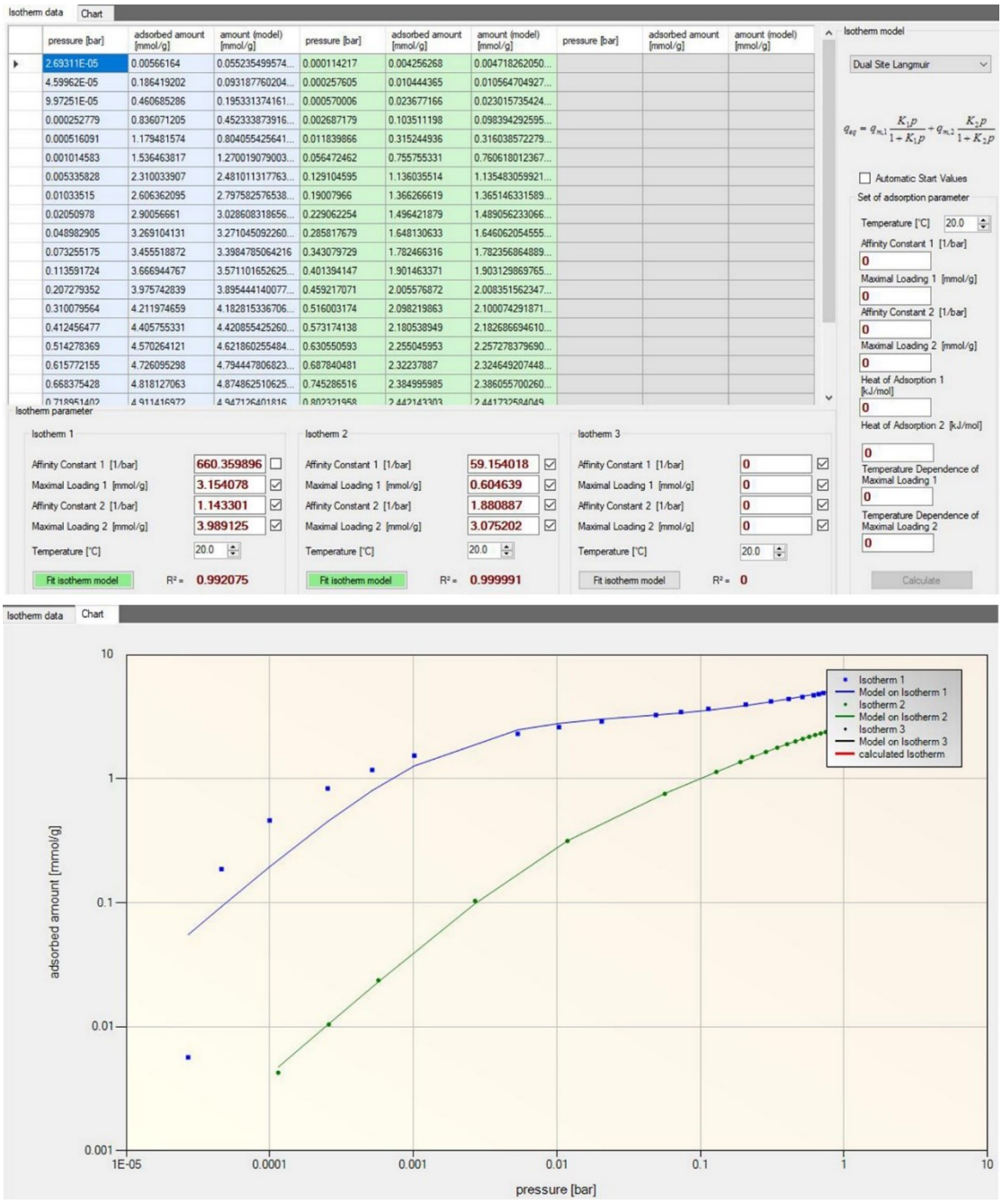

Fig. S16 The revised isotherm parameters of SO_2 and CO_2 re-fitted by Dual Site Langmuir model (top) by omitting the data below 0.01 bar which gave an 'Affinity constant 1' for SO_2 of 660 bar^{-1}. The corresponding fitting results of chart with log(x) and log(y) for better visualization (bottom).

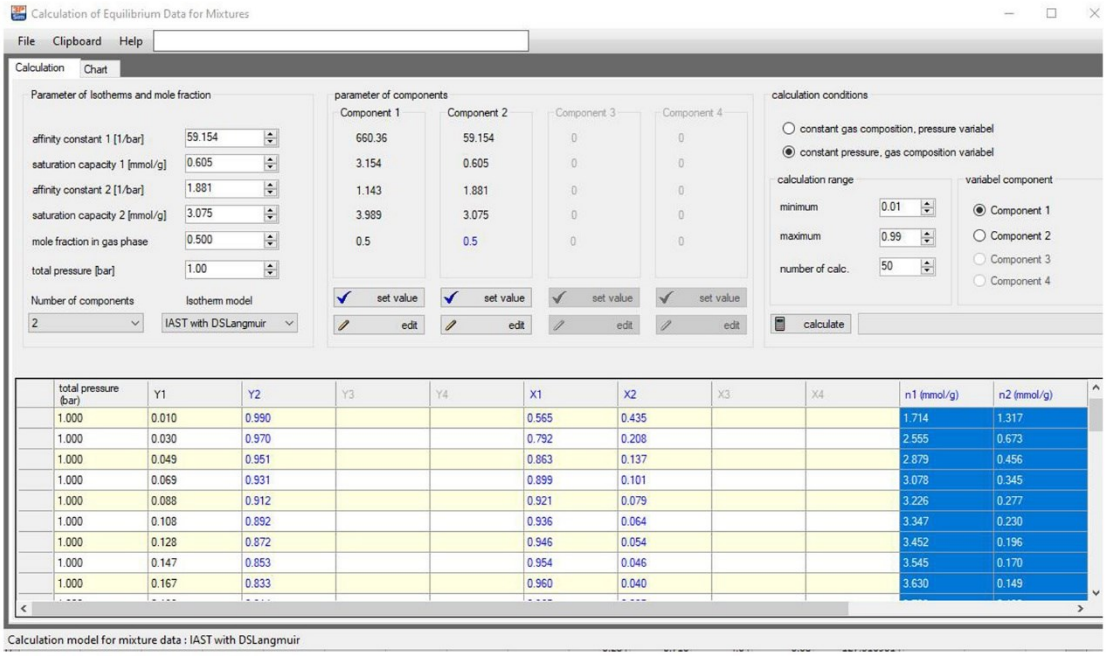

=($N8/$O8)/($L8/$M8)

F	G	H	I	J	K	L	M	N	O	P
						molar fraction				
						y1	y2	x1 (mmol/g)	x2(mmol/g)	IAST selectivity
						0.01	0.99	1.714	1.317	128.8428246
						0.03	0.97	2.555	0.673	122.7513621
						0.049	0.951	2.879	0.456	122.5353115
						0.069	0.931	3.078	0.345	120.378828
						0.088	0.912	3.226	0.277	120.6970791
						0.108	0.892	3.347	0.23	120.1901771
						0.128	0.872	3.452	0.196	119.9834184
						0.147	0.853	3.545	0.17	121.0038015
						0.167	0.833	3.63	0.149	121.5203151
						0.186	0.814	3.709	0.133	122.0440618
						0.206	0.794	3.783	0.119	122.5300645
						0.226	0.774	3.852	0.107	123.2920354
						0.245	0.755	3.918	0.097	124.4725437
						0.265	0.735	3.98	0.088	125.441681
						0.284	0.716	4.04	0.08	127.3169014
						0.304	0.696	4.097	0.073	128.4927902
						0.324	0.676	4.151	0.067	129.2646029
						0.343	0.657	4.204	0.061	132.0091765
						0.363	0.637	4.254	0.057	130.9650573
						0.382	0.618	4.303	0.052	133.8730366
						0.402	0.598	4.35	0.048	134.8103234
						0.422	0.578	4.395	0.044	136.8111805
						0.441	0.559	4.438	0.041	137.2071235
						0.461	0.539	4.481	0.038	137.8729878
						0.48	0.52	4.522	0.035	139.9666667
						0.5	0.5	4.561	0.032	142.53125

Fig. S17 The IAST prediction calculation result for SO_2/CO_2 mixture based on the revised fitted isotherm parameters from the fit presented in Fig. S16 (top). The IAST SO_2/CO_2 selectivity result (bottom) with molar fraction as the x axis and IAST selectivity as y axis are plotted in Fig. 3a, main text.

In the initial calculation, the parameters were automatically obtained as the isotherm data appeared well fitted with the Dual Site Langmuir, DSLAI model. **Fig. S15** shows the previous fitting results of SO_2 and CO_2 isotherm data at 293 K up to 0.97 bar. The x and y axis are in logarithmic mode to visualize the fitting results at low pressure more clearly, and even the low-pressure data below 0.01 bar were fitted reasonably well and were included in the fit. We noticed that uncertainties could exist at the low-pressure range, and the very high 'Affinity constant 1' for SO_2 of 1321 bar^{-1} was caused by the very steep adsorption curve below 0.01 bar (58 $cm^3\ g^{-1}$ at 7.6 Torr).

In a modified fit, the isotherm data of each gas below 0.01 bar were omitted, with the remaining data fitted

with the DSLAI model to obtain parameters for the '3P sim' software by which we re-calculated the IAST selectivities for SO_2/CO_2, SO_2/CH_4 and SO_2/N_2. By omitting the data below 0.01 bar, the 'Affinity constant 1' for SO_2 changed to about 660 bar^{-1} (see **Fig. S16**). In addition, as shown in **Fig. S17**, the IAST selectivity calculation process for SO_2/CO_2 is shown based on the equation (4) in the ESI†. As a result, a IAST selectivity of 120 at SO_2:CO_2 (10:90, v:v) could still be obtained, which highlighted the potential of nanoCB6-H for SO_2 separation. Accordingly, the IAST selectivities of SO_2/CH_4 and SO_2/N_2, and breakthrough simulation have also been recalculated.

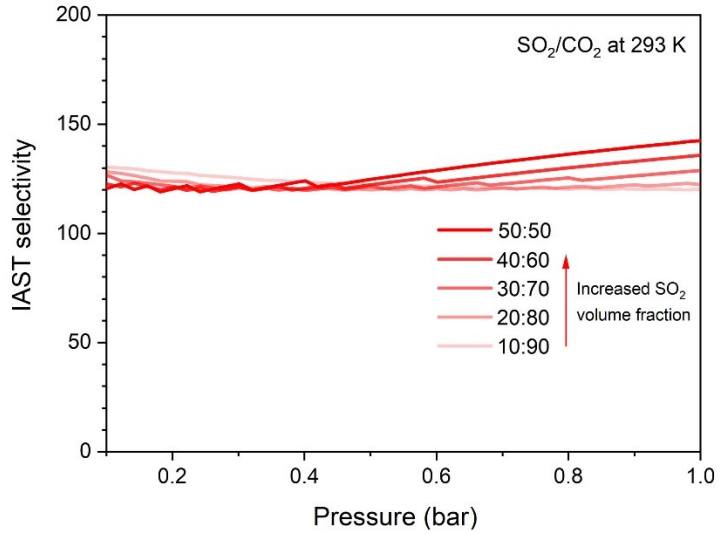

Fig. S18 IAST selectivities of recycled nanoCB6-H for SO_2/CO_2 mixtures with varying volume ratio from 10:90 to 50:50 (v/v) (light to dark colour) at 293 K. IAST calculations at low pressure (< 0.1 bar) carry large uncertainties due to the insufficient integration of spreading pressure and thus are not reported.

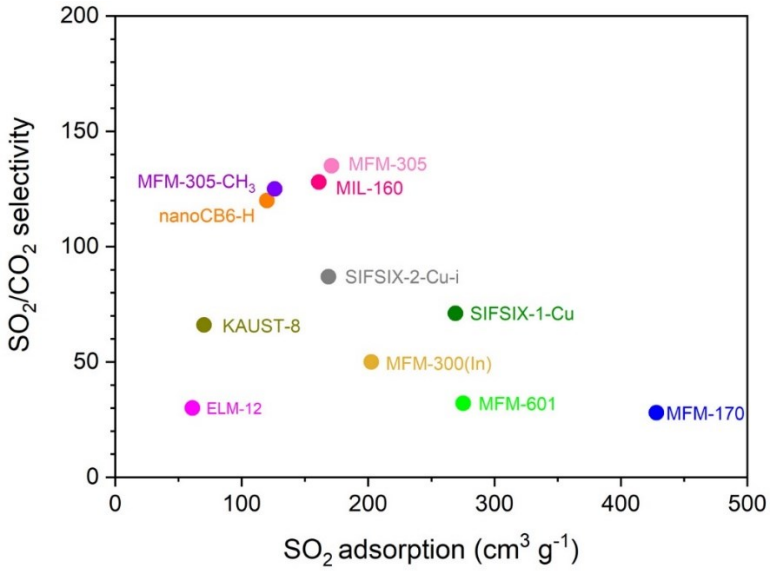

Fig. S19 SO_2/CO_2 selectivity of recycled nanoCB6-H and representative MOFs for gas mixtures with specific SO_2:CO_2 molar ratio (between 0.05:99.95 and 10:90) at 1.0 bar (details in Table S6). Plot of SO_2/CO_2 selectivity (at 1.0 bar and 298 K) against SO_2 adsorption. Temperature for nanoCB6-H and MIL–160 is at 293 K.

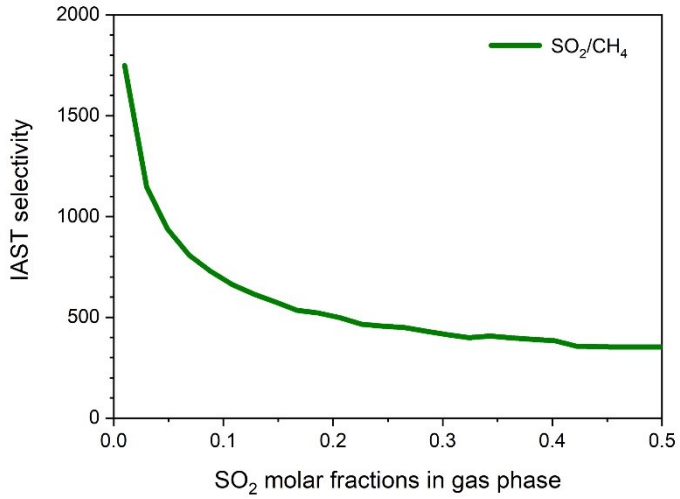

Fig. S20 IAST selectivities of recycled nanoCB6-H for SO_2/CH_4 mixtures with varying SO_2 molar fractions in the gas phase at 293 K and 1 bar.

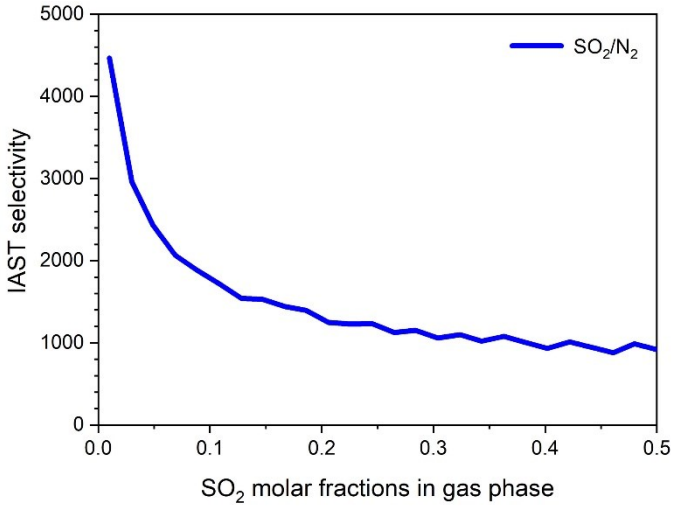

Fig. S21 IAST selectivities of recycled nanoCB6-H for SO_2/N_2 mixtures with varying SO_2 molar fractions in the gas phase at 293 K and 1 bar.

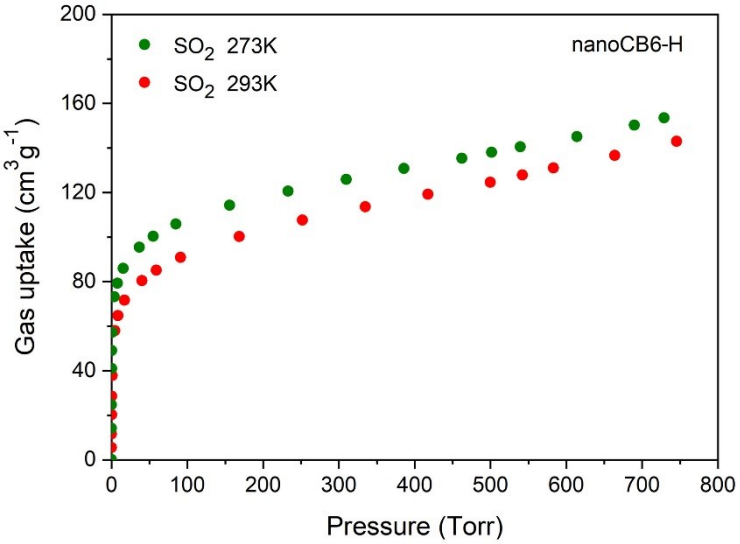

Fig. S22 SO_2 adsorption isotherms (the first runs) of newly activated nanoCB6-H from the same batch measured up to 1 bar at 273 K and 293 K, respectively.

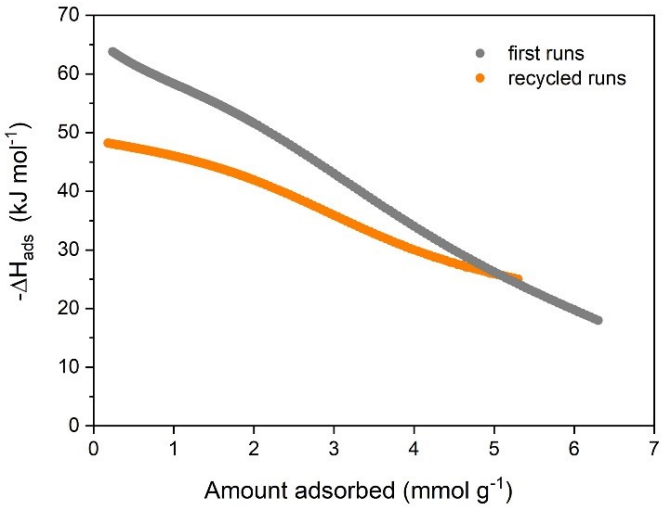

Fig. S23 Isosteric heat of adsorption of SO_2 for newly activated nanoCB6-H materials (grey) based on the first runs data, and recycled nanoCB6-H materials (brown) based on the recycled 7th and 8th runs data.

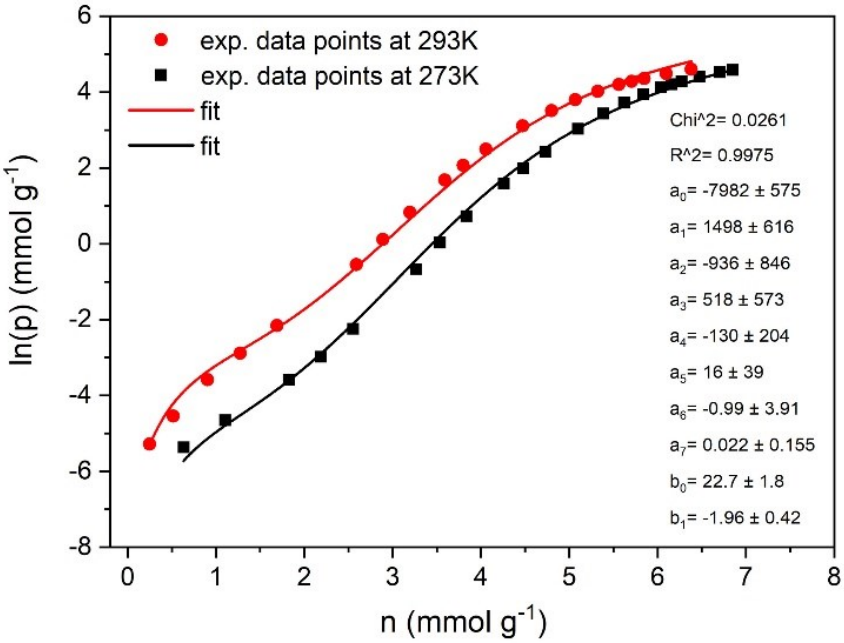

Fig. S24 Virial analysis of the SO_2 sorption data from the first runs with newly activated nanoCB6-H samples.

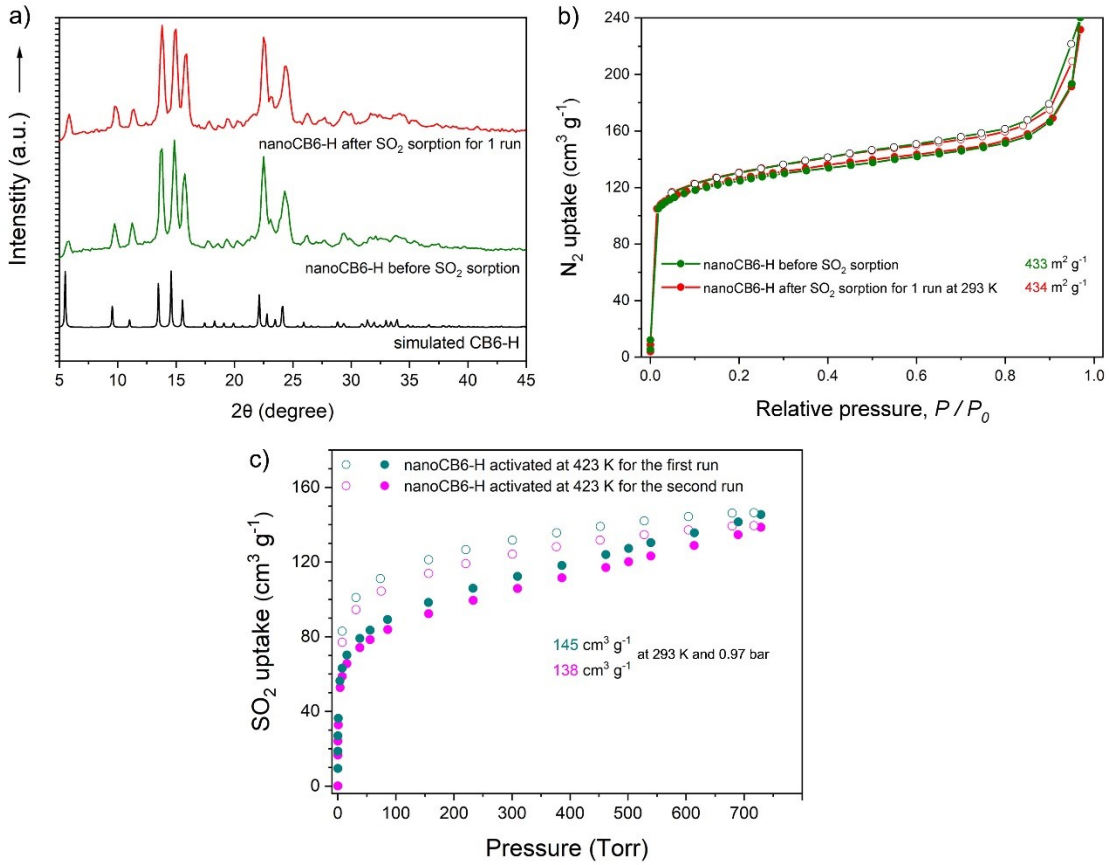

Fig. S25 a) PXRD patterns, b) N_2 sorption isotherms (77 K) of nanoCB6-H before and after SO_2 sorption for the first run at 293 K. c) The SO_2 sorption isotherms of nanoCB6-H for the first and second runs. Note: nanoCB6 was activated at 150 °C under a dynamic vacuum for 2 days.

There are factors, such as thermal treatment, interactions between SO_2 and the framework, and residual water molecules, which can affect the BET surface areas of HOFs. If there is residual water in the HOF, the possibility is high for the formation of "H_2SO_3", HSO_3^-, SO_3^{2-}, H_3O^+ etc., which is detrimental to the hydrogen-bonded

supramolecular framework during SO_2 adsorption. Thus, we did control experiments to investigate the effect of residual water molecules on the surface areas and SO_2 uptake of nanoCB6-H. The control experiment indicated that residual water molecules in nanoCB6-H could have led to the decreased surface areas after SO_2 sorption. According to the literature, the water guest molecules in CB6-based solids could not be totally removed at 100 °C under a dynamic vacuum for two days,[7] which was the same condition used for nanoCB6-H, $C_{36}H_{36}N_{24}O_{12}\cdot 1.8H_2O$, in our manuscript. However, guest-free porous CB6-H could be prepared by evacuation of the guest molecules inside the channels at 150 °C under a dynamic vacuum for two days reported by Kim.[1b] Thus, we prepared water-free nanoCB6-H by activating at 150 °C under a dynamic vacuum for two days, and tested N_2 sorption at 77 K before and after SO_2 sorption up to 0.97 bar at 293 K (Fig. S25). The results showed that water-free nanoCB6-H retained the unchanged BET surface areas (434 $m^2\ g^{-1}$) after one run of SO_2 sorption, and the SO_2 uptake values were still within experimental error of 145 $cm^3\ g^{-1}$ and 138 $cm^3\ g^{-1}$ for the first and the second run at 293 K and 0.97 bar. This enhanced behavior by water-free nanoCB6-H over that of nanoCB6-H with residual water (Fig. 3b), indicated that the removal of residual water molecules should avoid the possible formation of "sulfurous acid" etc. during SO_2 sorption, which is detrimental to the HOF, and led to decreased BET surface areas after SO_2 sorption. We tried to use FT-IR to detect the sulfurous acid species in nanoCB6-H with residual water after SO_2 sorption but failed due to the low amount.

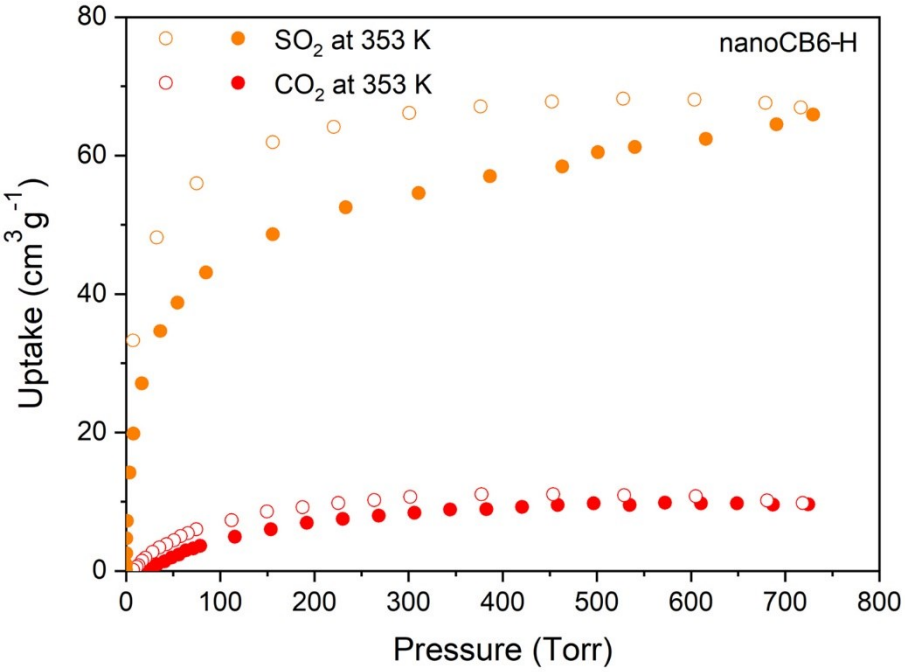

Fig. S26 SO_2 and CO_2 uptake isotherms of recycled nanoCB6-H samples measured up to 0.97 bar at 353 K, respectively. Filled and empty symbols represent adsorption and desorption, respectively.

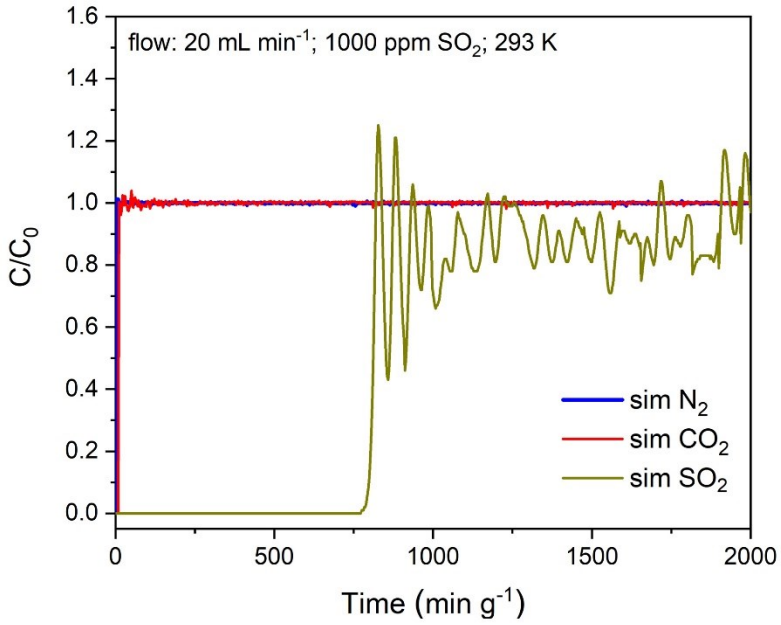

Fig. S27 Simulated breakthrough curves for recycled nanoCB6-H with $SO_2/CO_2/N_2$; 0.1/15.0/84.9; v:v:v at 293 K.

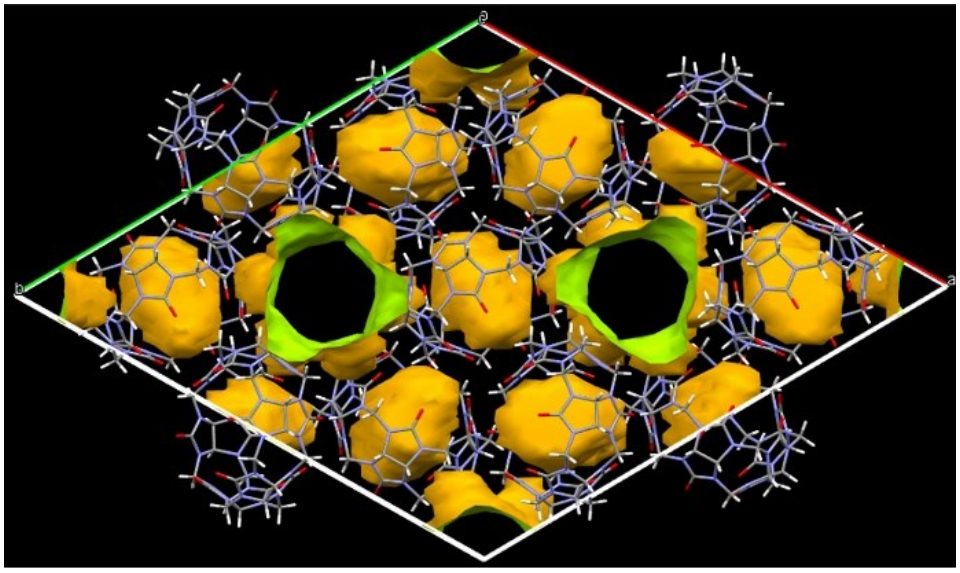

Fig. S28 Chemical view of the void volume of CB6-H based on the accessible surface in a unit cell with a probe 1.2 Å and 0.7 Å in mercury software.

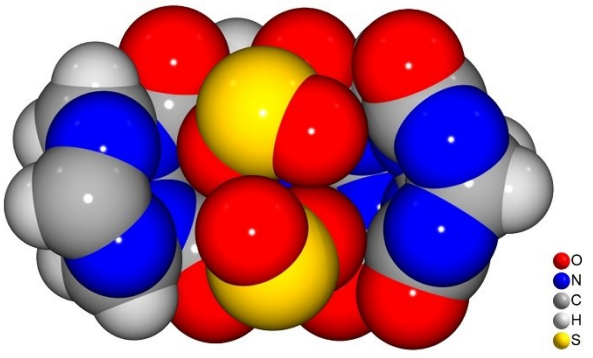

Fig. S29 Chemical view of a pair of SO_2 molecules encapsulated in the intrinsic pore of a CB6 cage. CB6 is partially drawn for clarity.

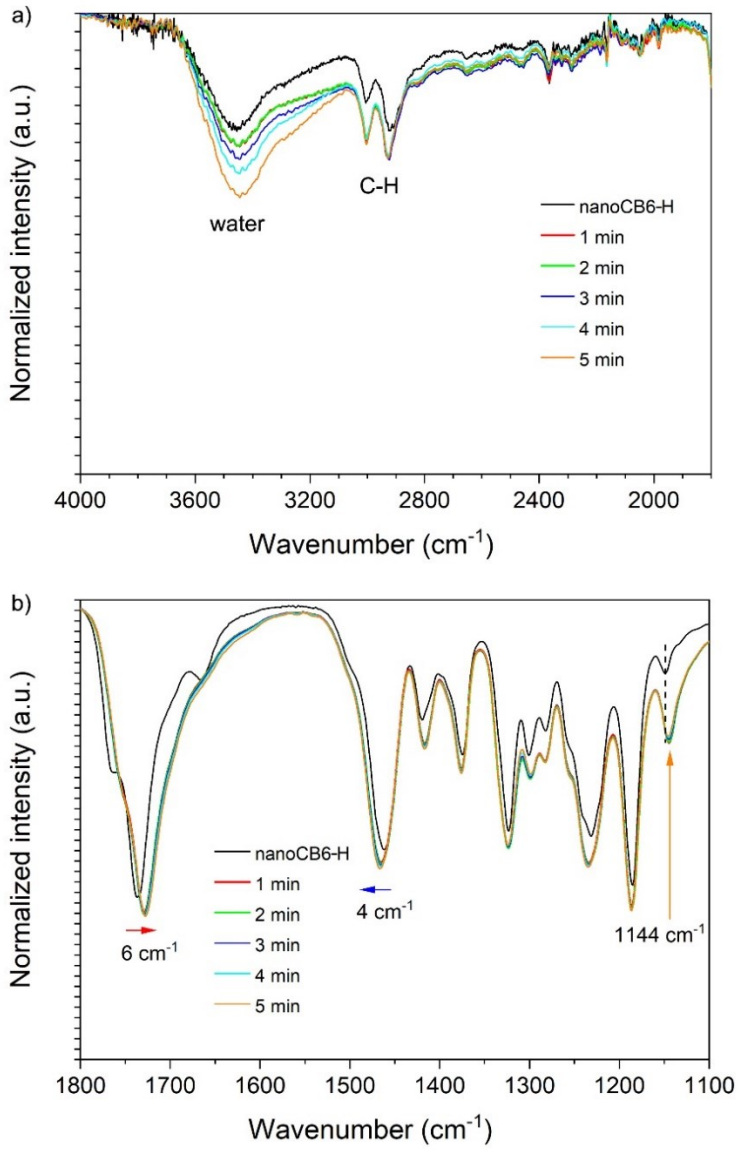

Fig. S30 FTIR spectra of nanoCB6-H and nanoCB6-H after uptake of SO_2 under atmosphere condition.

In Fig. S30a, the intensity of water signals is increasing when SO_2@nanoCB6-H is exposed to air for a certain time. In Fig. S30b, a new band at 1144 cm^{-1} is assigned to the V_1 symmetric stretch of adsorbed SO_2. IR signal peaks corresponding to carbonyl and methylene groups are redshifted and blue-shifted, respectively.

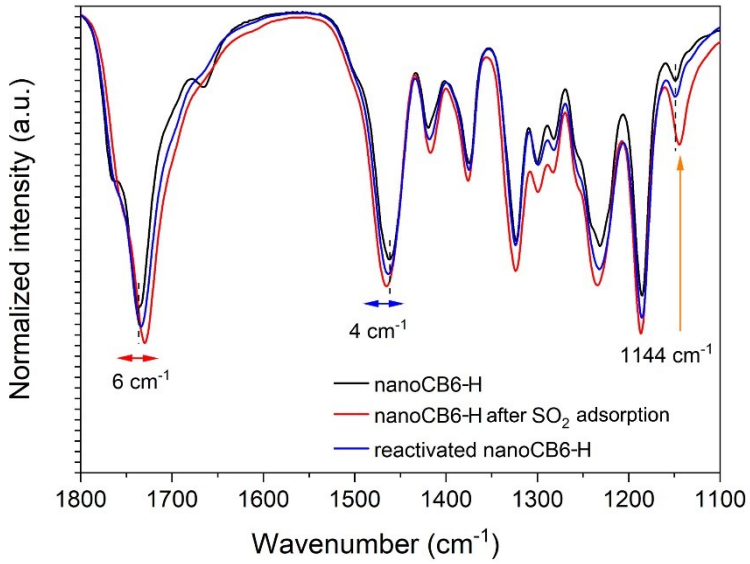

Fig. S31 FTIR spectra of nanoCB6-H, nanoCB6-H after uptake of SO_2, and the reactivated nanoCB6-H materials.

In Fig. S31 the reversible shifted peaks in nanoCB6-H and the disappearance of SO_2 signals in the reactivated nanoCB6-H indicate the release of SO_2 and the successful regeneration of materials.

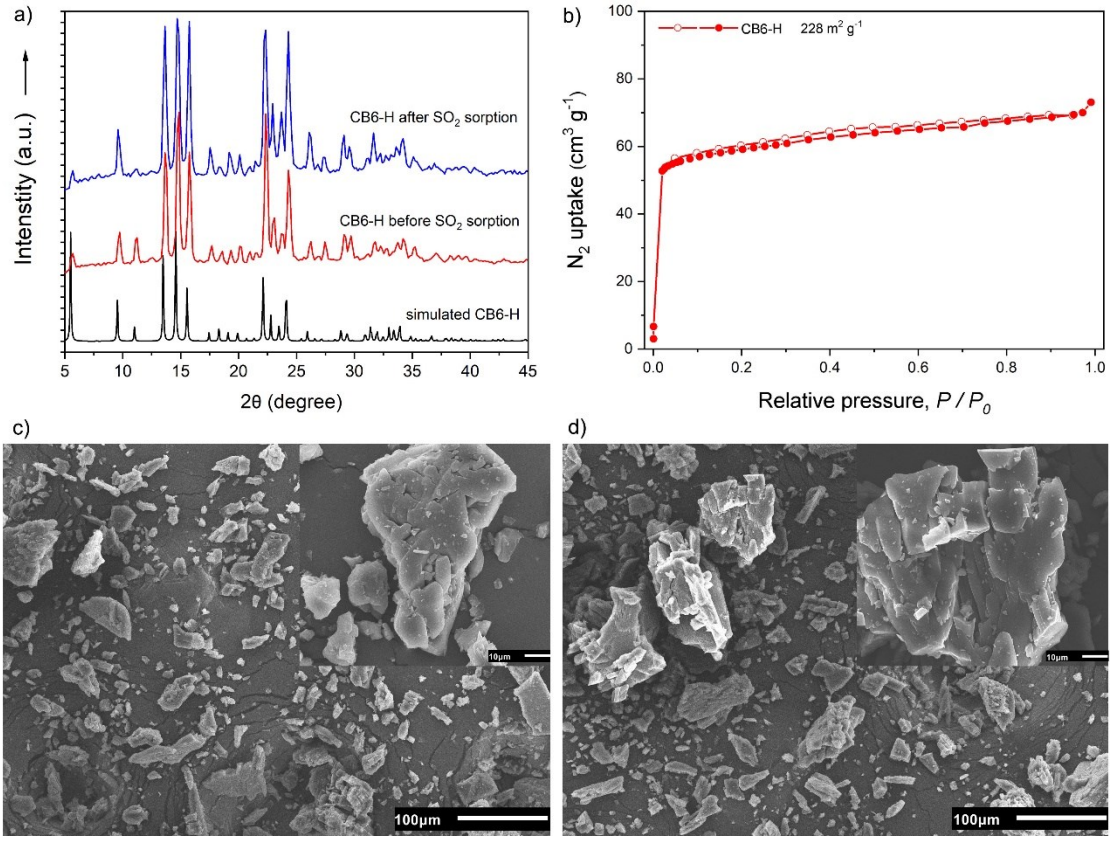

Fig. S32 a) PXRD patterns of CB6-H before and after SO_2 uptake at 293 K up to 0.97 bar. b) N_2 adsorption isotherms (77 K) of CB6-H. SEM images of CB6-H c) before and d) after SO_2 uptake at 293 K up to 0.97 bar.

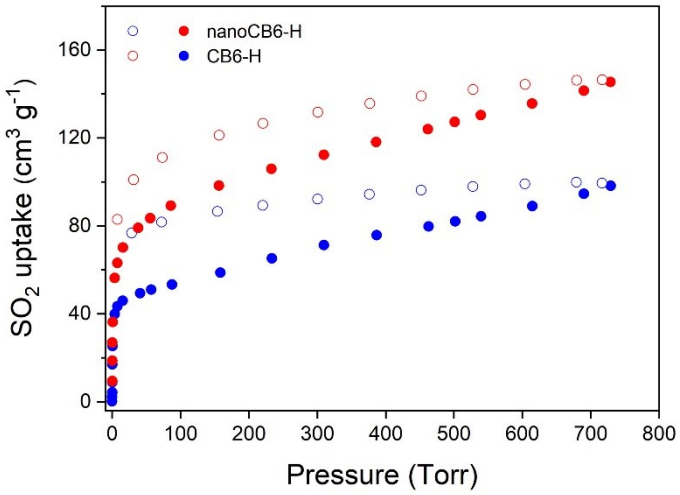

Fig. S33 Comparison of SO_2 sorption isotherms of nanoCB6-H and CB6-H up to 0.97 bar at 293 K for the first runs. Filled and empty symbols refer to adsorption and desorption, respectively.

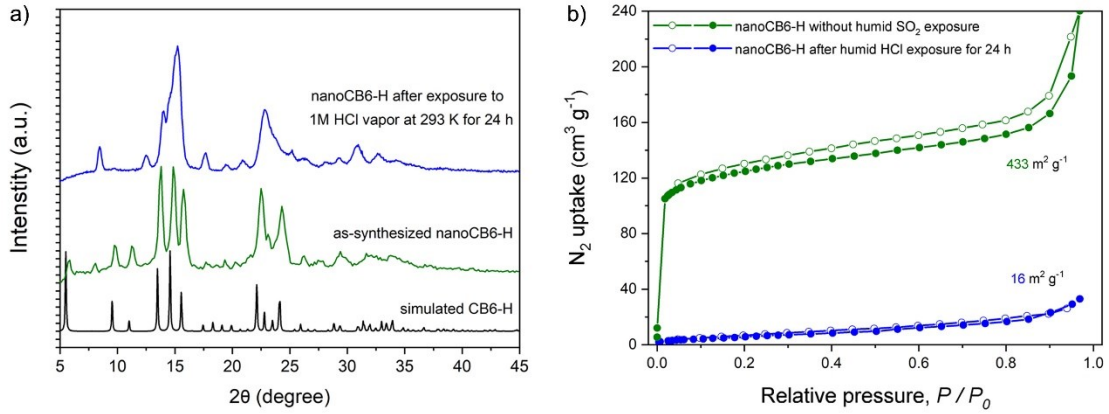

Fig. S34 a) PXRD patterns and b) N_2 adsorption isotherms (77 K) of nanoCB6-H before and after exposure to humid HCl.

Activated nanoCB6-H powders (36 mg) in a small glass bottle were exposed to humid HCl atmosphere provided by 1 M HCl aqueous solution at room temperature for 24 hours. After that, the PXRD data of treated sample was collected, and the sample was further activated at 373 K for 48 hours before N_2 sorption at 77 K was measured. It is observed that the crystalline phase of nanoCB6-H has deteriorated and also changed to another unknown phase with very low BET surface areas (16 $m^2\ g^{-1}$) (Fig. S34), which indicates the extrinsic pores between CB6 cages in the HOF are almost lost under the humid acidic atmosphere.

S4. Table S1–S7

Table S1. Textural properties of nanoCB6-H before and after dry SO_2 adsorption.

Sample	S_{BET} [a] ($m^2\,g^{-1}$)	Langmuir surface area ($m^2\,g^{-1}$)	Total pore volume [b] ($cm^3\,g^{-1}$)	Micropore volume [c] ($cm^3\,g^{-1}$)	note
nanoCB6-H	441	545	0.22	0.13	before SO_2 sorption
nanoCB6-H	383	514	0.21	0.088	after SO_2 sorption for ten runs at 293 K
CB6-H	228	-	0.10	0.070	before SO_2 sorption

[a] BET surface area was determined over 7 points in the relative pressure range P/P_0 = 0.05 − 0.08 from N_2 sorption isotherms at 77K.
[b] Total pore volumes (V_{total}) were determined from N_2 sorption isotherms at 77 K (p/p_0 = 0.90) for pores ≤ 20 nm diameter.
[c] Micropore volumes were determined using the t–plot method from five adsorption points in the pressure range P/P_0 = 0.1 − 0.2 based on N_2 adsorption curves at 77 K.

Table S2. Experimental results of gas adsorption in recycled nanoCB6-H.

SO_2 (cm^3/g) (mmol/g) mmol/mmol wt%	CO_2 (cm^3/g) (mmol/g) mmol/mmol wt%	CH_4 (cm^3/g) (mmol/g) mmol/mmol –	N_2 (cm^3/g) (mmol/g) mmol/mmol –	T (K)	Q_{st}^0 (SO_2) kJ mol^{-1}	Q_{st}^0 (CO_2) kJ mol^{-1}	Q_{st}^0 (CH_4) kJ mol^{-1}	Q_{st}^0 (N_2) kJ mol^{-1}
119.8	58	13.3	5.5	293	48	34.6	24.1	11.3
4.98	2.41	0.55	0.22					
4.96	2.40	0.55	0.22					
31.87	10.60	—	—					
138.6	70.3	19.2	7.5	273				
6.18	3.13	0.85	0.33					
6.16	3.12	0.85	0.33					
39.58	13.77	—	—					

Table S3. Parameters for DSLAI modelling on different gas adsorption isotherm of recycled nanoCB6-H.

Gas	Temp. (K)	Model	R^2	affinity const. 1 (1/bar)	max loading 1 (mmol/g)	affinity const. 2 (1/bar)	max loading 2 (mmol/g)
SO_2	293	DSLAI	0.992	660.360	3.154	1.143	3.989
CO_2	293	DSLAI	0.999	59.154	0.605	1.881	3.075
CH_4	293	DSLAI	0.999	3.698	0.245	0.056	7.835
N_2	293	DSLAI	0.999	2.401	0.073	0.028	7.455

Table S4. IAST selectivity results of different gas mixtures for recycled nanoCB6-H at 293 K and 1 bar.

Sample	IAST selectivity[a]			
	SO_2/CO_2 (10:90)	SO_2/CH_4 (10:90)	SO_2/N_2 (10:90)	CO_2/CH_4 (10:90)
nanoCB6-H	120[a]	662[a]	1720[a]	25[a]
	120[b]	684[b]	1754[b]	25[b]

[a] Constant pressure with varied molar ratios.

[b] Constant molar ratio with varied pressure.

Table S5. SO_2 sorption and separation properties of nanoCB6-H and other representative adsorbents.

sample	S_{BET} ($m^2\ g^{-1}$)	SO_2 uptake ($cm^3\ g^{-1}$)		Temp. (K)	SO_2/CO_2 (molar ratio, x : y)	Q_{st}^0	ref.
		0.1 bar	1 bar				
POCs							
nanoCB6-H	441	88	143.0[a]	293	–	64[a]	this
	383	81	121.2[b]	293	120 (10 : 90)[c]	48	work
CB6-H	228	50	98	293	-	-	this work
amorphous CB7	293[d]	54	105	297	–	–	8
mPEI/ASPOC composite	nonporous	–	12.9[e]		–	–	9
COFs							
COF–6	750	–	168.5[f]	303	40 (0.05 : 99.95)	31	10
PI–COF–m20	548	–	137.0	298	–	–	11
PI–COF–m40	279	–	134.5	298	–	–	11
PILs							
P([VBIm]Br)	nonporous	–	196.5	298	–	–	12
[IRA–900][$B(Im)_4$]	13	255	268.9	293	–	50.6[h]	13
Zeolites							
MFI zeolite	713	61.1[f]	68.5[f]	298		14	14

Note: [a] Data based on the first adsorption runs. [b] Data based on the 10th run of recycled nanoCB6-H. [c] Data based on IAST calculations. [d] Calculated from the isotherm of CO_2 at 196 K. [e] Determined gravimetrically with 200 ppm SO_2 in N_2 as the feed mixture. [f] SO_2 uptake capacity estimated from isotherm. [h] Interaction energy based on DFT calculations.

Table S6. SO_2 sorption and separation properties of representative MOF adsorbents.

sample	S_{BET} ($m^2\ g^{-1}$)	SO_2 uptake ($cm^3\ g^{-1}$)		Temp. (K)	SO_2/CO_2 (x : y)	Q_{st}^0	ref.
		0.1 bar	1 bar				
MFM–170	2408	153[a]	428.1	298	28 (1 : 99)[b]	–	15
ELM–12	706	43.7	61.2	298	30 (10 : 90)	78	16
MFM–601	3644	112	275.5	298	32 (10 : 90)	38	17
MFM–300(In)	1071	171.2	202.5	298	50 (10 : 90)	34.5	18
KAUST–8	258	39.7	70.3[a]	298	66 (0.05 : 99.95)[c]	73.9[d]	19
SIFSIX–1–Cu	1178	213.8	269.3	298	71 (10 : 90)	36.1	20
SIFSIX–2–Cu–i	630	147.0	168.8	298	87.1 (10 : 90)	38.1	20
SIFSIX–3–Zn	250	46.2	51.3	298	–	45.2	20
oxamato–based 3D MOF–2	1460	–	–	303	100 (2.5 : 97.5)	–	21
MIL–160	1070	123.2	161.0	293	128 (10 : 90)	42	22
MFM–305–CH3	256	107.6	126.2	298	125 (5 : 95)	32	23
MFM–305	779	122.3	171.0	298	135 (5 : 95)	39	23
HHU–2–Br	620	–	147.9	293	–		24
MFM–300(Al)	–	–	129.6	298	–	–	25
Prussian blue analogues CoCo	712	–	61.1	298	–	–	26
Prussian blue analogues ZnCo	700	13.3	44.0	298	–	–	26
FMOF–2	378	10.8	43.7	298	–	–	27

Note: [a] SO_2 uptake capacity estimated from isotherm. [b] Data based on IAST calculations. [c] Data based on breakthrough experiment result. [d] Interaction energy based on DFT calculations.

Table S7. Representative non–covalent bonds between CB6 cage and SO_2 molecules, and bonding energies based on DFT calculations.

Bond type	Bond length (Å)	Bonding energies (kJ mol^{-1})
Site I		–50.3
S—O	2.69	
S—O	3.01	
(SO_2) O—H	2.19	
Site II		–59.5
S—O	3.00	
S—O	3.02	
Site III		–82.4
S—O	3.03	
S—O	3.04	
(SO_2) O—C=O	3.13	
(SO_2) O—C=O	3.15	
S—O (SO_2)	3.40	
S—O (SO_2)	3.40	
Site IV		–49.7
(SO_2) S—O	2.63	
(SO_2) O—C=O	2.97	
(SO_2) S—N	3.52	
(SO_2) S—N	3.65	
(SO_2) O—H	2.64	
Site V		–18.8
(SO_2) O—H	2.49	
(SO_2) O—H	2.51	
(SO_2) O—H	2.80	
(SO_2) O—H	2.85	

S5. References

1 a) J. Tian, J. Liu, J. Liu and P. K. Thallapally, *CrystEngComm*, 2013, **15**, 1528–153; b) J. H. Park, K. Suh, M. R. Rohman, W. Hwang, M. Yoon and K. Kim, *Chem. Commun*., 2015, **51**, 9313–9316; c) J. Liang, A. Nuhnen, S. Millan, H. Breitzke, V. Gvilava, G. Buntkowsky and C. Janiak, *Angew. Chem. Int. Ed.*, 2020, **59**, 6068-6073.

2 a) 3P INSTRUMENTS, 3P sim, Version 1.1.0.7, Simulation and Evaluation Tool for mixSorb, 3P INSTRUMENTS 2018; b) A. Möller, R. Eschrich, C. Reichenbach, J. Guderian, M. Lange and J. Möller, *Adsorption* 2017, **23**: 197–209; c) C. A. Grande, R. Blom, A. Möller and J. Möller, *Chem. Eng. Sci*., 2013, **89**, 10–20.

3 M. J. Frisch, G. W. Trucks, H. B. Schlegel, G. E. Scuseria, M. A. Robb, J. R. Cheeseman, G. Scalmani, V. Barone, G. A. Petersson, H. Nakatsuji, X. Li, M. Caricato, A. V. Marenich, J. Bloino, B. G. Janesko, R. Gomperts, B. Mennucci, H. P. Hratchian, J. V. Ortiz, A. F. Izmaylov, J. L. Sonnenberg, D. Williams-Young, F. Ding, F. Lipparini, F. Egidi, J. Goings, B. Peng, A. Petrone, T. Henderson, D. Ranasinghe, V. G. Zakrzewski, J. Gao, N. Rega, G. Zheng, W. Liang, M. Hada, M. Ehara, K. Toyota, R. Fukuda, J. Hasegawa, M. Ishida, T. Nakajima, Y. Honda, O. Kitao, H. Nakai, T. Vreven, K. Throssell, J. A. Montgomery, Jr., J. E. Peralta, F. Ogliaro, M. J. Bearpark, J. J. Heyd, E. N. Brothers, K. N. Kudin, V. N. Staroverov, T. A. Keith, R. Kobayashi, J. Normand, K. Raghavachari, A. P. Rendell, J. C. Burant, S. S. Iyengar, J. Tomasi, M. Cossi, J. M. Millam, M. Klene, C. Adamo, R. Cammi, J. W. Ochterski, R. L. Martin, K. Morokuma, O. Farkas, J. B. Foresman, and D. J. Fox. *Gaussian 16, Revision A.03*; Gaussian, Inc., Wallingford CT, 2016.

4 K. I. Assaf and W. M. Nau, *Chem Soc Rev*., 2015, **44**, 394–418.

5 S. Grimme, J. Antony, S. Ehrlich and H. Krieg, *J. Chem. Phys*. 2010,**132**, 154104–154122.

6 S. F. Boys and F. Bernardi, *Mol. Phys*.1970,**19**, 553–566.

7 S. Lim, H. Kim, N. Selvapalam, K.-J. Kim, S. J. Cho, G. Seo and K. Kim, *Angew. Chem*. Int. Ed., 2008, **120**, 3400–3403.

8 J. Tian, S. Ma, P. K. Thallapally, D. Fowler, B. P. McGrail and J. L. Atwood, *Chem. Commun.,* 2011, **47**, 7626–7628.

9 G. Zhu, J.–M. Y. Carrillo, A. Sujan, C. N. Okonkwo, S. Park, B. G. Sumpter, C. W. Jones and R. P. Lively, *J. Mater. Chem. A*, 2018, **6**, 22043–22052.

10 H. Wang, X. Zeng, W. Wang and D. Cao, *Chem. Eng. Sci.*, 2015, **135**, 373–380.

11 G. Y. Lee, J. Lee, H. T. Vo, S. Kim, H. Lee and T. Park, *Sci. Rep.*, 2017, **7**, 557.

12 L. Xia, Q. Cui, X. Suo, Y. Li, X. Cui, Q. Yang, J. Xu, Y. Yang and H. Xing, *Adv. Funct. Mater.,* 2018, **28**, 1704292.

13 X. He, X. Lv, X. Fan, W. Lin, H. Li and C. Wang, *Acta Phys.–Chim. Sin.*, 2018, **34**(8), 896–903.

14 I. Matito–Martos, A. Martin–Calvo, J. J. Gutierrez–Sevillano, M. Haranczyk, M. Doblare, J. B. Parra, C. O. Ania and S. Calero, *Phys. Chem. Chem. Phys.*, 2014, **16**, 19884–19893.

15 G. L. Smith, J. E. Eyley, X. Han, X. Zhang, J. Li, N. M. Jacques, H. G. W. Godfrey, S. P. Argent, L. J. McCormick McPherson, S. J. Teat, Y. Cheng, M. D. Frogley, G. Cinque, S. J. Day, C. C. Tang, T. L. Easun, S. Rudic, A. J. Ramirez–Cuesta, S. Yang and M. Schröder, *Nat. Mater.,* 2019, **18**, 1358–1365.

16 Y. Zhang, P. Zhang, W. Yu, J. Zhang, J. Huang, J. Wang, M. Xu, Q. Deng, Z. Zeng and S. Deng, *ACS Appl. Mater. Interfaces,* 2019, **11**, 10680–10688.

17 J. H. Carter, X. Han, F. Y. Moreau, I. da Silva, A. Nevin, H. G. W. Godfrey, C. C. Tang, S. Yang and M. Schröder, *J. Am. Chem. Soc.*, 2018, **140**, 15564–15567.

18 M. Savage, Y. Cheng, T. L. Easun, J. E. Eyley, S. P. Argent, M. R. Warren, W. Lewis, C. Murray, C. C. Tang, M. D. Frogley, G. Cinque, J. Sun, S. Rudic, R. T. Murden, M. J. Benham, A. N. Fitch, A. J. Blake, A. J. Ramirez–Cuesta, S. Yang and M. Schröder, *Adv. Mater.*, 2016, **28**, 8705–8711.

19 M. R. Tchalala, P. M. Bhatt, K. N. Chappanda, S. R. Tavares, K. Adil, Y. Belmabkhout, A. Shkurenko, A. Cadiau, N. Heymans, G. De Weireld, G. Maurin, K. N. Salama and M. Eddaoudi, *Nat. Commun.,* 2019, **10**, 1328.

20 X. Cui, Q. Yang, L. Yang, R. Krishna, Z. Zhang, Z. Bao, H. Wu, Q. Ren, W. Zhou, B. Chen and H. Xing, *Adv. Mater.*, 2017, **29**, 1606929.

21 M. Mon, E. Tiburcio, J. Ferrando–Soria, R. Gil San Millan, J. A. R. Navarro, D. Armentano and E. Pardo, *Chem.*

Commun., 2018, **54**, 9063–9066.

22 P. Brandt, A. Nuhnen, M. Lange, J. Mollmer, O. Weingart, C. Janiak, *ACS App. Mater. Interfaces* 2019, **11**, 17350–17358.

23 L. Li, I. da Silva, D. I. Kolokolov, X. Han, J. Li, G. Smith, Y. Cheng, L. L. Daemen, C. G. Morris, H. G. W. Godfrey, N. M. Jacques, X. Zhang, P. Manuel, M. D. Frogley, C. A. Murray, A. J. Ramirez–Cuesta, G. Cinque, C. C. Tang, A. G. Stepanov, S. Yang, M. Schroder, *Chem Sci* 2019, **10**, 1472–1482.

24 T. Matemb Ma Ntep, H. Breitzke, L. Schmolke, C. Schlüsener, B. Moll, S. Millan, N. Tannert, I. El Aita, G. Buntkowsky, C. Janiak, *Chem. Mater.,* 2019, **31**, 8629–8638.

25 X. Han, H. G. W. Godfrey, L. Briggs, A. J. Davies, Y. Cheng, L. L. Daemen, A. M. Sheveleva, F. Tuna, E. J. L. McInnes, J. Sun, C. Drathen, M. W. George, A. J. Ramirez–Cuesta, K. M. Thomas, S. Yang and M. Schröder, *Nat. Mater.*, 2018, **17**, 691–696.

26 P. K. Thallapally, R. K. Motkuri, C. A. Fernandez, B. P. McGrail and G. S. Behrooz, *Inorg. Chem.*, 2010, **49**, 4909–4915.

27 C. A. Fernandez, P. K. Thallapally, R. K. Motkuri, S. K. Nune, J. C. Sumrak, J. Tian and J. Liu, *Cryst. Growth Des.*, 2010, **10**, 1037–1039.